CrystEngComm

Single crystal growth, transport and scanning tunneling microscopy and spectroscopy of FeSe1-xSx

Journal:	*CrystEngComm*
Manuscript ID	CE-ART-01-2018-000074.R1
Article Type:	Paper
Date Submitted by the Author:	23-Feb-2018
Complete List of Authors:	Chareev, Dmitriy; Russian Academy of Sciences, Institute of Experimental Mineralogy Ovchenkov, Yevgeniy; M.V.Lomonosov Moscow State University , Faculty of Physics Shvanskaya, Larisa; Lomonosov Moscow State University, Crystallography and Crystal Chemistry Kovalskii, Andrey; National University of Science and Technology "MISIS", Inorganic nanomaterials Abdel-Hafiez, Mahmoud; Physikalisches Institut Johann Wolfgang Goethe-Universität Traine, Dan; Temple University Department of Physics Lechner, Eric; Temple University Department of Physics Iavarone, Maria; Temple University, Physics Volkova, Olga; M.V. Lomonosov Moscow State University, Low Temperature Physics Department of Physics Faculty; Vasiliev, Alexander; M.V. Lomonosov Moscow State University, Low Temperature Physics Department of Physics Faculty

Journal Name

ARTICLE

Single crystal growth, transport and scanning tunneling microscopy and spectroscopy of FeSe1-xSx

Received 00th January 20xx,
Accepted 00th January 20xx

DOI: 10.1039/x0xx00000x

www.rsc.org/

Dmitriy Chareev,[a,b,c] Yevgeniy Ovchenkov,[d] Larisa Shvanskaya,[d,e] Andrey Kovalskii,[e] Mahmoud Abdel-Hafiez,[e,f,g] Dan J. Trainer,[h] Eric M. Lechner,[h] Maria Iavarone,[h] Olga Volkova[b,d,i] and Alexander Vasiliev*[d,e,i]

Single crystals of sulfur-substitued iron selenide, $FeSe_{1-x}S_x$, were grown within eutectics of molten halides, $AlCl_3$/KCl, $AlCl_3$/KCl/NaCl or $AlCl_3$/KBr, at permanent temperature gradient. The innovative "ampoule in ampoule" design of a crystallization vessel allows obtaining the mm-sized plate-like single crystals with the sulfur content up to x ~ 0.19. The sharp anomalies in physical properties mark the superconducting at T_C = 8.4 K and nematic at T_N = 90 K phase transitions in $FeSe_{0.96}$. Scanning tunneling microscopy reveals presence of dumbbell defects associated with Fe vacancies and dark defects at the chalcogen site associated to S within $FeSe_{1-x}S_x$ series of compounds. Scanning tunneling spectroscopy shows the presence of two different superconducting gaps at both hole and electron pockets of Fermi surface for low level of S content. As a function of sulfur content, TC follows the conventional dome-shaped curve while T_N decreases with x. The overall appearance of T - x phase diagram in $FeSe_{1-x}S_x$ suggests the importance of nematic fluctuations for the formation of superconducting state in these compounds.

Introduction

Iron selenide, $FeSe_{1-\delta}$, exhibits intriguing and distinctive properties, which are currently in the research focus in the field of high temperature superconductors. This binary compound undergoes tetragonal-to-orthorhombic transition at about 90 K[1] and possesses an electronic nematic order below this temperature similar to many other Fe-based parent materials. However, no magnetic order is formed at ambient pressure[2] and it becomes superconducting at about 8-9 K.[3] It shows superconductivity in a nearly stoichiometric form and stays a Pauli paramagnet down to lowest temperatures. The superconducting transition temperature of this material can be increased (to 15-27 K) by pressure[4] and reaches over 45 K in a nanoscale FET type device.[5] This places iron selenide on the verge of high temperature superconductivity and stimulates interest to study related and substituted series. Among these, the isovalent substitution of Se by S is supposed to produce a mild distortion of the crystal structure being, therefore, of considerable interest. The synthesis of $FeSe_{1-x}S_x$ single crystals up to the highest possible concentration of sulfur is considered to be an important part of the comprehensive research of Fe based superconductors as this system allows investigating the relationship between superconductivity and nematicity. Indeed, nematicity can be systematically suppressed by the isovalent S substitution. Moreover, sulfur substitution to FeSe enhances the upper critical field H_{C2} and the critical current density. T_C initially increases slightly to $T_C \approx 11$ K at S ~ 10% from $T_C \approx 8.5$ K at x = 0, but then decreases.[6]

There are several experiments that have explored the electronic properties of $FeSe_{1-x}S_x$. Angle-resolved photoemission spectroscopy (ARPES) measurements[7,8] have revealed that the size of the Fermi surface increases and that the anisotropy decreases by increasing x. An anisotropic superconducting gap was reported by ARPES in the 4% substituted sample[9] but, in general, the x ranges studied so far are very limited.

According to the phase diagram of the Fe-Se system, superconducting tetragonal $FeSe_{1-\delta}$ coexists with metallic iron and h-$Fe_{1-\Delta}Se$ hexagonal phase.[10] At 457 °C tetragonal phase decomposes by the peritectoid reaction $FeSe_{1-\delta}$ = h-$Fe_{1-\Delta}Se$ + Fe. Homogeneity region of $FeSe_{1-x}$ is very narrow, the range of possible compositions is from $FeSe_{0.96}$ to $FeSe_{0.975}$.[11] $FeS_{1-\delta}$, isostructural to FeTe and FeSe (P4/nmm; *a* = 3.674 Å, *c* = 5.033 Å), is a mineral, mackinawite.[12] The exact composition of both natural and synthetic mackinawite is unknown and its thermodynamic stability has not been proven. Natural mackinawite decomposes forming pyrrotite at 120 – 135 °C.[13,14] The superconductivity of synthetic mackinawite was described in Ref. 15. The low stability of mackinawite makes

[a] Institute of Experimental Mineralogy, RAS, Chernogolovka 123456, Russia
[b] Ural Federal University, Ekaterinburg 620002, Russia
[c] Kazan Federal University, Kazan 420008, Russia
[d] Lomonosov Moscow State University, Moscow 119991, Russia
E-mail: vasil@mig.phys.msu.ru; Tel & fax: +7 495 932 92 17
[e] National University of Science and Technology "MISiS", Moscow 119049, Russia
[f] Goethe University Frankfurt, Frankfurt am Main 60438, Germany
[g] Fayoum University, Fayoum 63514, Egypt
[h] Temple University, Philadelphia, PA 19122, USA
[i] National Research South Ural State University, Chelyabinsk 454080, Russia
DOI: 10.1039/x0xx00000x

difficult the synthesis of stable $Fe(Se_{1-x}S_x)_{1-\delta}$ solid solutions, especially at large x.

Although phase relations within mixture of FeSe and FeS are not studied in details, it is known that the tetragonal iron selenide with any sulfur content is in equilibrium with metallic iron at any temperature. Taking into account that FeSe decomposes at 457 °C, and tetragonal FeS is possibly not stable one can explain the absence of complete sulfur-for-selenium substitution in FeSe. Thus, the temperature of synthesis of iron selenide should not exceed 457 °C, and the maximum temperature of synthesis of tetragonal $Fe(Se,S)_{1-\delta}$ solid solution should decrease with the increase of sulfur content.

Experimental section

A technique chosen for the growth of $Fe(Se,S)_{1-\delta}$ crystals was synthesis in eutectic molten metal chlorides under permanent temperature gradient.[16,17] Molten chlorides constitute a very low melting eutectic mixture $AlCl_3$/KCl ($K_1Al_2Cl_7$), $AlCl_3$/KCl/NaCl ($Na_{0.5}K_{0.5}Al_2Cl_7$) or $AlCl_3$/KBr ($K_1Al_2Cl_6Br_1$). The permanent gradient is formed when the quartz ampoule with the chalcogen feed and the mixture of haloid salts is placed into a furnace and the temperatures at the ends of the ampoule are different due to the ampoule position. The feed gradually dissolves in the hot end of the ampoule and deposits in the cold end in the form of single crystals. The major advantage of this technique is that physical and chemical parameters of crystal growth are strictly specified and constant in time unlike the classical solution-melt technique, when the multicomponent system gradually cools producing the single crystals.[18] Previously, this method has been used to obtain high quality crystals of superconducting iron selenide $FeSe_{1-\delta}$.[19]

To grow the single crystals of sulfur substituted iron selenite the feed of $Fe_{1.3}Se_{1-x}S_x$ composition, x = 0.05-0.40, was synthesized. A stable excess of iron increases the chemical potential of iron in the system preventing the formation of hexagonal h-$Fe_{1-\Delta}(Se,S)$.

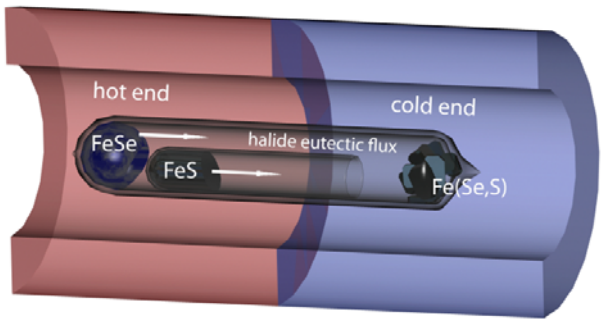

Fig. 1. "Ampoule in ampoule" design for crystal growth of $FeSe_{1-x}S_x$. The temperature decreases from the left (hot) end to the right (cold) end.

Sometimes, pieces of metallic iron were added to the cold end of the ampoule to increase its chemical potential. This also leads to conditions suitable for formation of tetragonal rather than hexagonal iron chalcogenides. To avoid possible mutual influence of sulfur and selenium ions during migration from the hot end of the ampoule to the cold end the "ampoule in the ampoule" design was employed, as shown in Fig. 1. This approach was advanced earlier to grow coexisting single crystals of FeAsS + FeS_2 where As and S migration routes were separated and (Fe,Ni)Te crystals with Fe and Ni separation.[20]

The feed of bulk composition of $Fe_{1.3}Se$ was placed into a thick-walled ampoule of 11 mm in inner diameter while the feed of $Fe_{1.3}S$ was placed into an open thin-walled ampoule of 8 mm in outer diameter. Then, anhydrous $AlCl_3$ was added to single or double ampoules followed by air-stable alkali halides, e.g. KBr or KCl-NaCl mixture. Small amounts of these salts slightly decrease the melting point of aluminum chloride and prevent melting and evaporation of aluminum chloride during evacuation and sealing of the ampoules. The ampoules were placed into tube furnaces so that the end with no feed was at the edge of the furnace in order to create the temperature gradient of about 50 – 100°C. The furnaces were slowly heated to 400 – 420°C and then were left under these conditions for 7-8 weeks. Since the solubility range of sulfur in iron selenide strongly depends on the crystallization temperature, the ampoules longer than 150mm sometimes were used.

Fig. 2. Secondary electron images of a $FeSe_{0.96}S_{0.04}$ single crystal. (a) $FeSe_{0.96}S_{0.04}$ single crystal; (b) tridimensional Fe(Se,S) crystal; (c) Fe_2Si (dark-gray) on the boundaries of Fe(Se,S) crystals (light-gray).

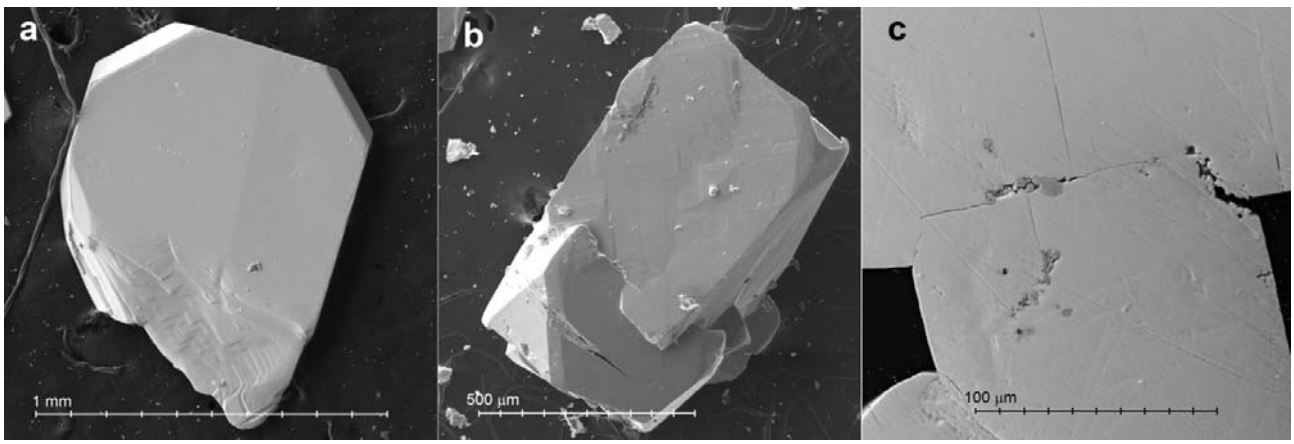

Double ampoules often exploded during heating, sometimes with detonation of the other ampoules. To prevent this ampoules were heated in two stages: on the first day up to 250 °C, on the second day up to the final temperature of synthesis. During the night the melted aluminum chloride had sufficient time to dissolve other salts which decreased its vapor pressure. Moreover, it was noticed that the explosion may be prevented by using the feed in the form of compressed pellets of the corresponding size instead of powder. Synthesized crystals were washed from molten salts in water, then in ethanol and afterwards in acetone using the ultrasonic bath and then were dried for a short time in dry boxes at 70 °C and. As shown in Fig. 2, flat tetragonal crystals of about the mm in lateral size and thickness of about tenths of μm were obtained in all single ampoules where the sulfur content in the feed did not exceed 20 %. In the ampoules with higher sulfur content the hexagonal magnetic crystals were obtained routinely or no transport of substance was observed. The crystals were stored in vacuum.

In double ampoules tetragonal crystals (Fig. 2a) or less often hexagonal crystals (see Fig.S1 of Supplementary) were also found. In each ampoule the tetragonal crystals were either flat indistinguishable in shape from those grown in single ampoules or tridimensional, which often formed co-oriented sintered crystals (Fig. 2b). The difference in crystal shape can be explained by different degrees of supersaturation of the molten salt due to the interaction of dissolved ions of selenium and sulfur. In sintered Fe(Se,S) crystals particles of the approximate composition Fe2Si, up to 10μm in size (Fig. 2c) were often found. Usually sulfur content was from 2 to 19%, but in one experiment a millimeter-size crystal containing 22 ± 1% of sulfur was found among small crystals. Microprobe analysis has shown that tetragonal crystals had an insignificant excess of iron compared to the combined content of sulfur and selenium. No impurity elements (Al, K, Na, Cl, Br) were found. The sulfur content in tetragonal crystals was always approximately two times lower than that in the feed. The use of long ampoules does not help to increase the sulfur content in the samples but increased the total amount of transported substance.

The dependence of the ratio of iron to the sum of selenium and sulfur on the sulfur content (Fe/(Se+S) vs. S) was studied for the crystals of five different compositions by microprobe analysis. It was observed that the iron to chalcogens ratio remains constant within the error limits. It was the same as in pure tetragonal iron selenide and equals 0.92±0.04. The difference in non-stoichiometry obtained in this study and studies dealing with powder samples (~0.96) can be explained by the systematic error of X-ray fluorescence microanalysis or by oxidation of the surface of the polished crystal.

The lattice constants were determined by an Xcalibur-S area detector diffractometer with Mo K_α radiation. According to the single-crystal X-ray characterization all the samples are beloning to the tetragonal phase with lattice constants close to those reported for the polycrystalline samples of $FeSe_{1-\delta}$.[21] Fig. 3 presents the variation of lattice constants *a* and *c* in the $FeSe_{1-x}S_x$ samples. XRD pattern of $FeSe_{0.9}S_{0.1}$ is shown in Fig.S2 of Supplementary. Our data show that the substitution of Se by S results in decrease of both in-plane lattice parameter *c* and inter-plane lattice parameter *a*. The crystal lattice parameters within $FeSe_{1-x}S_x$ series of compounds are collected in Table S1 of Supplementary. Similar results have been reported for powder $FeSe_{1-x}S_x$ (0.1<x<0.5) samples.[22]

Scanning tunneling microscopy and spectroscopy

Low temperature scanning tunneling microscopy (STM) and spectroscopy (STS) measurements have been performed using a Unisoku UHV STM system, with a base pressure of 4×10^{-11} Torr. The crystals were cleaved in UHV at room temperature and soon after were transferred to the STM scanner at low temperature. Pt-Ir tips were used in all experiments.

Atomically resolved images were acquired in the constant current mode. STM topography image acquired at the surface of a pure FeSe single crystal at T =1.5 K is shown in the left panel of Fig. 4. The image reveals the presence of dimer-like defects (bright spots) surrounded by dark regions that are usually associated to Fe vacancies.[23] Similar dumbbell defects have also been imaged in other FeSe crystals grown by vapor transport.[24,25]

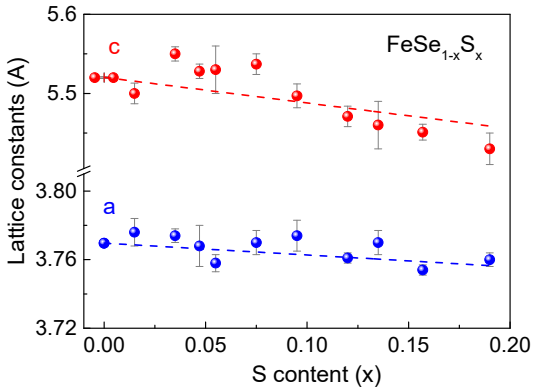

Fig. 3. The lattice constants a and c of the Fe(Se1-xSx)1-δ tetragonal single crystals as a function of S content. The data values for parent compound FeSe1- δ are taken from Ref. [15].

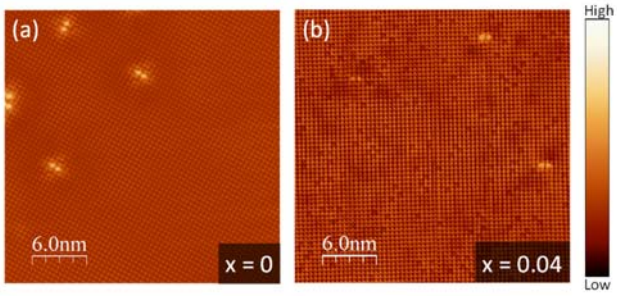

Fig. 4. (a) Constant-current STM image of a cleaved (001) FeSe single crystal. Scanning parameters are V = 25mV and I = 60 pA. The scanning direction is at approximately 45 degrees with the topmost Se atoms. (b) STM image of FeS0.04Se0.96. Scanning parameters are V = -20mV and I = 100 pA. The scanning direction is almost parallel to the topmost Se lattice. In both images scan area is 23.5 nm x 23.5 nm.

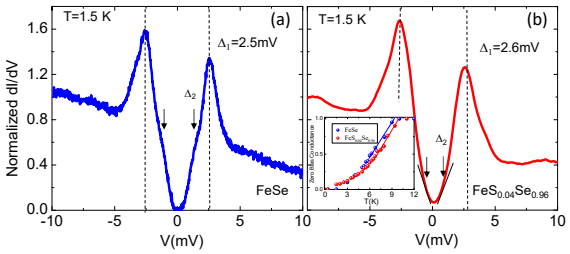

Fig. 5. Tunneling spectra dI/dV acquired at T=1.5 K (a) on FeSe and (b) $FeS_{0.04}Se_{0.96}$. Tunneling conditions are V=10 mV, I=60 pA, lock-in modulation V_{mod}=0.2 mV and lock-in frequency f=373.1 Hz. The tunneling spectra have been normalized to V=-10 mV. The inset in (b) is the evolution of zero bias conductance as a function of temperature for the two samples and shows a shift at higher temperature in the critical temperature of the $FeS_{0.04}Se_{0.96}$ sample.

They are aligned both along the *a*- and *b*-axis, which point to their independence from a structural orthorhombic distortion.[26] STM topography image acquired at the surface of a $FeSe_{0.96}S_{0.04}$ single crystal is shown in the right panel of Fig 4. Also in this case dumbbell defects are present with a similar concentration. Dark defects at the chalcogen site are associated with the S atoms that have smaller radii than the Se atoms. The density of these defects corresponds closely to the nominal concentration of sulfur in the measured sample. These kind of defects are absent in the pure FeSe sample.

Conductance spectra, dI/dV, which are proportional to the local electronic density of states, have been acquired using the lock-in *ac* modulation technique while the I-V curves were recorded simultaneously. A typical tunneling spectrum acquired on the surface of FeSe at T=1.5 K is shown in the left panel of Fig. 5. The spectrum presents clear coherence peaks at Δ_1=± 2.5 meV that have been observed in other STM measurements both on thin films[27,28] and on single crystals.[24,25,29] This gap is usually associated to the gap present on the Γ-pocket, as the tunneling probability is much higher for tunneling into the Γ hole-pocket. Another feature is also present in the spectrum as a kink at lower energy Δ_2=± 1.1 meV, and we associate this to the gap of the electron-pocket. A typical spectrum acquired on a $FeSe_{0.96}S_{0.04}$ single crystal at T=1.5 K is shown in the right panel of Fig. 5. The spectrum presents coherence peaks corresponding to the Γ hole-pocket at slightly higher energy (Δ_1=2.6 meV) and the lower energy feature at slightly lower energy (Δ_2=± 0.9 meV).

In order to extract the superconducting transition temperatures we plotted the zero bias conductance (ZBC) as a function of temperature in the inset to right panel of Fig. 5 for both samples. The ZBC of the tunneling spectra is the electronic density of states at the Fermi level. As the temperature increases and the gap closes the ZBC value increases to 1 in the normal state. Taking the intersection point of two straight lines, that fit the ZBC values in the range 6-9 K and the higher temperature region, we can estimate the transition temperature Tc. We find that the transition temperature increases from the pure sample to the 4% S substituted sample by about 1 K. While the transition temperatures determined with this method might not be precise, they show a clear trend in agreement with the transport data.

At low S substitutions (4%) we find that the spectroscopic features associated to the Γ-hole gap and that of the electron pocket are almost unchanged in within the thermal broadening of the tunneling spectrum. These results are in agreement with previous findings reported on similar substitution levels by STM[30] and ARPES.[9] This suggests that at low S substitution levels the strength of the superconducting pairing is not significantly affected by the initial suppression of the nematic order and the reduced anisotropy of the Fermi surface reported by ARPES.[7]

Phase diagram

Overall composition – temperature phase diagram is shown in Fig. 6. The temperature of superconducting phase transition T_C was determined in measurements of magnetization, specific heat and resistivity.[6,31,32] In the range *x*=0-0.19, the composition dependence of superconducting transition temperature exhibits conventional dome shape. The temperature of nematic phase transition, determined by position of kink on *R*(*T*), decreases with a sulfur content in agreement with Ref. 28. For *x* = 0.037, the temperature dependence of resistivity is shown in the inset to Fig. 6. At *x* = 0.19 the singularity on *R*(*T*) was not detected reflecting the full suppression of nematic phase transition.

No long-range magnetic order can be observed at ambient pressure in $FeSe_{1-x}S_x$, which implies an isolated nematic quantum critical point.[33] It has been reported that the spin density wave order can also be induced in $FeSe_{1-x}S_x$ when physical pressure is applied.[34] However, at higher x, the spin density wave phase can be completely decoupled from the nematic phase under pressure. Therefore, the chemical pressure introduced by S substitution offers an important route to separate the effects of nematic and magnetic fluctuations, allowing a discussion of their relative influence on superconducting pairing.

Fig. 6. Temperature – composition phase diagram for $FeSe_{1-x}S_x$ series of compounds.

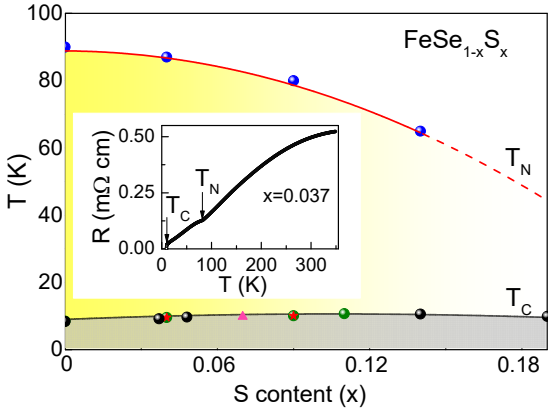

Conclusions

$FeSe_{1-x}S_x$ single crystals were obtained up to 19% of sulfur content using the innovative "ampoule in ampoule" techniqueof crystal growth under permanent gradient of temperature in the mixture of molted metal chlorides. This method allows obtaining large size high quality single crystals with a wide range of S-substitution levels. Non-stoichiometry does not depend strongly on the sulfur content and is the same as non-stoichiometry in tetragonal FeSe. Scanning tunneling microscopy reveals presence of dumbbell defects associated with Fe vacancies In the S-substituted crystals depressions are observed at the chalcogen lattice and are associated to Sulphur atoms that have a smaller radii than Selenium. Scanning tunneling spectroscopy evidences presence of two different superconducting gaps at both hole and electron pockets of Fermi surface that do not change significantly at low S-substitution (4%). As function of sulfur content, T_C follows the conventional dome-shaped curve while T_N decreases with x. The overall appearance of T-x phase diagram in $FeSe_{1-x}S_x$ suggests importance of nematic fluctuations at formation of superconducting state in these compounds.

Conflicts of interest

The authors contributed equally and declare no competing interests.

Acknowledgements

This work was supported by the Ministry of Education and Science of the Russian Federation in the framework of Increase Competitiveness Program of NUST "MISiS" grant K2-2017-084, by acts 211 of the Government of Russian Federation, Contracts No. 02.A03.21.0004, 02.A03.21.0006, 02.A03.21.0011 and by Russian Government Program of Competitive Growth of Kazan Federal University. The work in Germany was supported by the program MO30214/2. The work at Temple University, where low temperature scanning tunneling measurements were performed, was supported by U.S. Department of Energy under Grant No. DE-SC0004556.

References

1. T.M. McQueen, A.J. Williams, P.W. Stephens, J. Tao, Y. Zhu, V. Ksenofontov, F. Casper, C. Felser and R.J. Cava, *Phys. Rev. Lett.*, 2009, **103**, 057002.
2. Y. Mizuguchi and Y. Takano, *J. Phys. Soc. Jpn.* **79**, (2010) 102001.
3. F.-C. Hsu, J.-Y. Luo, K.-W. Yeh, T.-K. Chen, T.-W. Huang, P. M. Wu,Y.-C. Lee, Y.-L. Huang, Y.-Y. Chu, D.-C. Yan and M.-K. Wu, *Proc.Natl. Acad. Sci. U.S.A.*, 2008, **105**, 14262.
4. Y. Mizuguchi, F. Tomioka, S. Tsuda, T. Yamaguchi and Y. Takano, *Appl. Phys. Lett.*, 2008, **93**, 152505.
5. B. Lei, J. H. Cui, Z. J. Xiang, N. Z. Wang, C. Shang, N.Z. Wang, G. J. Ye, X. G. Luo, T. Wu, Z. Sun and X.H. Chen, Phys. Rev. Lett. 2016, **116**, 077002.
6. M. Abdel-Hafiez, Y.-Y. Zhang, Z.-Y. Cao, C.-G. Duan, G. Karapetrov, V.M. Pudalov, V.A. Vlasenko, A.V. Sadakov, D. A. Knyazev, T.A. Romanova, D.A. Chareev, O.S. Volkova, A.N. Vasiliev and X.-J. Chen, *Phys. Rev. B*, 2015, **91**, 165109.
7. M.D. Watson, T.K. Kim, A.A. Haghighirad, S.F. Blake, N.R. Davies, M. Hoesch, T. Wolf and A.I. Coldea, *Phys. Rev. B*, 2015, **92**, 121108.
8. P. Reiss, M.D. Watson, T.K. Kim, A.A. Haghighirad, D.N. Woodruff, M. Bruma, S.J. Clarke and A.I. Coldea, *Phys. Rev. B*, 2017, **96**, 121103.
9. H.C. Hu, X.H. Niu, D.F. Hu, J. Jiang, Q. Yao, Q.Y. Chen, Q. Song, M. Abdel-Hafiez, D.A. Chareev, A.N. Vasiliev, Q.S. Wang, H.L. Wo, J. Zhao, R. Peng and D.L. Feng, *Phys. Rev. Lett.*, 2016, **117**, 157003.
10. H. Okamoto, *J. of Phase Equilibria*, 1991, **12**, 383.
11. F. Gronvold, *Acta Chem. Scand.*, 1968, **22**, 1219.
12. L.A.Taylor and L.W. Finger, *Carnegie Institute of Washington Geophys. Lab. Ann. Rept.*, 1970, **69**, 318.
13. H. Zoka, L.A. Taylor and S. Takeno, *J. Sci. Hiroshima Univ. C,*1973, **7**, 37.
14. D.J. Vaughan and J.R. Craig, *Mineral Chemistry of Metal Sulfides*, Cambridge Univ. Press, Cambridge (1978).
15. X. Lai, H. Zhang, Y. Wang, X. Wang, X. Zhang, J. Lin and F. Huang, *J. Am. Chem. Soc.*, 2015, **137**, 10148.
16. S.G. Parker and J.E. Pinnell, *J. Cryst. Growth*, 1968, **3**, 490.
17. J.-Q. Yan, B. C. Sales, M. A. Susner and M. A. McGuire, *Phys. Rev. Materials*, 2017, **1**, 023402.
18. R. Hu, H. Lei, M. Abeykoon, E.S. Bozin, S.J.L. Billinge, S. J., J.B. Warren, T. Sigrist and C. Petrovic, *Phys. Rev. B*, 2011, **83**, 224502.
19. D. Chareev, E. Osadchii, T. Kuzmicheva, J.-Y. Lin, S. Kuzmichev, O. Volkova and A. Vasiliev, *CrystEngComm*, 2013, **15**, 1989.
20. D.A. Chareev, O.S. Volkova, N.V. Geringer, A.V. Koshelev, A.N. Nekrasov, V.O. Osadchii, E.G. Osadchii and O.N. Filimonova, *Crystallography Reports*, 2016, ***61***, 682.
21. S. Margadonna, Y. Takabayashi, M.T. Mc.Donald, K. Kasperkiewics, Y. Mizuguchi, Y. Takano, A. N. Fitch, E. Suard and K. Prassides. *Chem. Commun.*, 2008, 5607.
22. Y. Mizuguchi, F. Tomioka, S. Tsuda, T. Yamaguchi and Y. Takano. *J. Phys. Soc. Jpn.* 2009, **78**, 074712.
23. D. Huang, T.A. Webb, C.-L. Song, C.-Z. Chang, J.S. Moodera, E. Kaxiras and J.E. Hoffman, *Nano Lett.*, 2016, **16**, 4224.
24. S. Kasahara, T. Watashige, T. Hanaguri, Y. Kohsaka, T. Yamashita, Y. Shimoyama, Y. Mizukami, R. Endo, H. Ikeda, K. Aoyama, T. Terashima, S. Uji, T. Wolf, H. von Lohneisen, T. Shibauchi and Y. Matsuda, *Proc. Natl. Acad. Sci. U.S.A.*, 2014, **111**, 16309.

25. T. Watashige, Y. Tsutsumi, T. Hanaguri, Y. Kohsaka, S. Kasahara, A. Furusaki, M. Sigrist, C. Meingast, T. Wolf, H. von Lohneysen, T. Shibauchi and Y. Matsuda, *Phys. Rev. X*, 2015, **5**, 031022.
26. T.M. McQueen, A.J. Williams, P.W. Stephens, J. Tao, Y. Zhu, V. Ksenofontov, F. Casper, C. Felser and R.J. Cava, *Phys. Rev. Lett.*, 2009, **103**, 057002.
27. C.-L. Song, Y.-L. Wang, P. Cheng, Y.-P. Jiang, W. Li, T. Zhang, Z. Li, K. He, L. Wang, J.-F. Jia, H.-H. Hung, C. Wu, X.-C. Ma, X. Chen and Q.-K. Xue, *Science,* (2011), **332**, 1410.
28. C.-L. Song, Y.-L. Wang, Y.-P. Jiang, L. Wang, K. He, X. Chen, J. E. Hoffman, X.-C. Ma and Q.-K. Xue, *Phys. Rev. Lett.*, 2012, **109**, 137004.
29. P.O. Sprau, A. Kostin, A. Kreisel, A.E. Bohmer, V. Taufour, P.C. Canfield, S. Mukherjee, P.J. Hirschfeld, B.M. Andersen and J.C. S. Davis, *Science*, 2017, **357**, 75.
30. S.A. Moore, J.L. Curtis, C. Di Giorgio, E. Lechner, M. Abdel-Hafiez, O.S. Volkova, A.N. Vasiliev, D.A. Chareev, G. Karapetrov and M. Iavarone, *Phys. Rev. B*, 2015, **92**, 235113.
31. M. Abdel-Hafiez, J. Ge, A.N. Vasiliev, D.A. Chareev, J. Van de Vondel, V.V. Moshchalkov and A.V. Silhanek, *Phys. Rev. B*, 2013, **88**, 174512.
32. M. Abdel-Hafiez, Y.J. Pu, J. Brisbois, R. Peng, D.L. Feng, D.A. Chareev, A.V. Silhanek, C. Krellner, A.N. Vasiliev and X.-J. Chen, *Phys. Rev. B*, 2016, **93**, 224508.
33. S. Hosoi, K. Matsuura, K. Ishida, H. Wang, Y. Mizukami, T. Watashige, S. Kasahara, Y. Masuda and T. Shibauchi, Proc. Natl. Acad. Sci. USA 2016, **113**, 8139.
34. K. Matsuura, Y. Mizukami, Y. Arai, Y. Sugimura, N. Maejima, A. Machda, T. Watanuki, T. Fukuda, T. Yajima, Z. Hiroi, K.Y. Yip, Y.C. Chan, Q. Niu, S. Hosoi, K. Ishida, K. Mukasa, S. Kasahara, J.G. Cheng, S.K. Goh, Y. Matsuda, Y. Uwatoko and T. Shibauchi, Nat. Comm. 2017, **8**, 1143.